THE JOURNAL OF PHYSICAL CHEMISTRY C

Article

Cite This: J. Phys. Chem. C 2018, 122, 9611−9618

pubs.acs.org/JPCC

Phonon Energy Dependent Energy Transfer Upconversion for the Red Emission in the Er^{3+}/Yb^{3+} System

Hao Wu,[†,‡] Zhengdong Hao,[*,†] Liangliang Zhang,[†] Xia Zhang,[†] Yu Xiao,[†,‡] Guo-Hui Pan,[†] Huajun Wu,[†] Yongshi Luo,[†] Haifeng Zhao,[†] and Jiahua Zhang[*,†]

[†]State Key Laboratory of Luminescence and Applications, Changchun Institute of Optics, Fine Mechanics and Physics, Chinese Academy of Sciences, Changchun 130033, China

[‡]University of Chinese Academy of Sciences, Beijing 100049, China

Supporting Information

ABSTRACT: The red emission through upconversion (UC) upon 980 nm excitation based on Er^{3+}/Yb^{3+} combination is very attractive for bioimaging applications. The intensity of the red emission is observed to be strongly dependent on the host materials. However, the origin of the behavior and the quantitative dependence remain unclear. Here, the effectiveness of the second step UC excitation from the Er^{3+} intermediate state $^4I_{13/2}$ to the $^4F_{9/2}$ level by energy transfer from Yb^{3+} is studied for three popular hosts (β-$NaYF_4$, $Ba_5Gd_8Zn_4O_{21}$, and Y_2O_3) that have different phonon energies. Their emission efficiencies of the red emitting state are calculated, and the radiative lifetime of the $^4F_{9/2}$ level in $Ba_5Gd_8Zn_4O_{21}$ is reported for the first time. We present a spectroscopic method to evaluate the relative energy transfer coefficients for the three hosts and find the coefficient increases markedly with the increase of phonon energy, reflecting the nature of phonon-assisted energy transfer. The coefficient for β-$NaYF_4$ is 89 and 408 times smaller than that for the other two oxide hosts, well revealing the origin of the green emission governed UC in β-$NaYF_4$ and the red emission in the other two. Accordingly, a comprehensive analysis of the luminescence dynamical processes shows that selecting material with appropriate phonon energy is essential for both effective excitation and efficient emission of the red level.

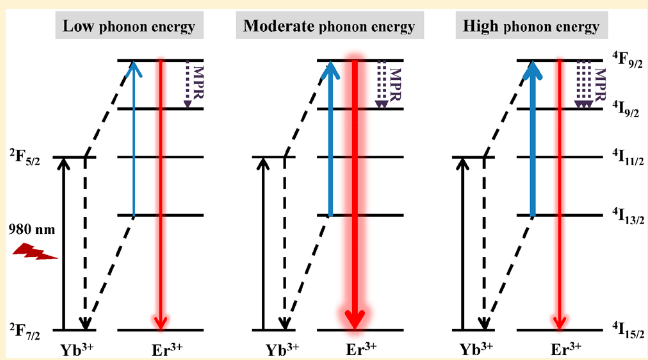

1. INTRODUCTION

Upconversion (UC) luminescence (UCL) in trivalent rare earth ion (RE^{3+})-doped materials[1−10] and semiconductors[11−13] has attracted massive attention owing to its unique luminescence characteristics and potential applications in UC lasers, biomarkers, drug delivery, 3D displays, optical temperature sensors, etc. Particularly, RE^{3+}-doped UCL nanomaterials show advantages of high resistance to color-fading, low toxicity, and minimal autofluorescence of organisms compared with traditional fluorescent probes in the bioimaging field, which has led to a great deal of research on UCL during the past few decades.[3,14,58,59] These materials can convert two or more low-energy photons into a high-energy photon. Typically, Er^{3+} ions are usually selected as activators of UC materials on account of their long-lived and abundant energy levels. In general, Yb^{3+} ions served as effective sensitizers in UC phosphors (UCPs), giving a high absorption cross-section around 980 nm, which matches well with the wavelength of inexpensive GaAs semiconductor lasers.[15] In the Er^{3+}/Yb^{3+} system, Er^{3+} ions may emit two visible UC emissions upon 980 nm excitation. One is a green emission centered at 550 nm originating from the $^4S_{3/2} \rightarrow {}^4I_{15/2}$ transition and the other one is a red emission centered at 660 nm corresponding to the $^4F_{9/2} \rightarrow {}^4I_{15/2}$ transition. Notably, the red emission wavelength of Er^{3+} locates within the so-called optical window (650−900 nm) of live biological tissues where light absorption and scattering are minimized.[16]

In order to look for efficient UCPs, a large number of works were deployed on materials having low phonon energies to inhibit multiphonon-relaxation (MPR) processes for enhancing UC quantum yields (UCQY).[17−19] Generally, fluorides are chosen to be suitable host materials for achieving highly efficient UCL because of their low phonon energies. Among various inorganic fluoride-based UCPs, hexagonal sodium yttrium fluoride (β-$NaYF_4$) is recognized to be one of the most efficient green UCPs owing to its multisite distribution (high disorder in structure) and low phonon energy (~360 cm^{-1}).[20−23] Besides, the rare earth sesquioxides have been widely studied because of their good stability and rather low phonon energies (~600 cm^{-1}) in oxide materials. Y_2O_3 is a sort of cubic sesquioxide, which can be prepared into single crystal or transparent ceramic, and is regarded as one of the ideal solid

Received: March 13, 2018
Revised: April 11, 2018
Published: April 13, 2018

Downloaded via CHANGCHUN INST OMP on July 23, 2019 at 07:49:17 (UTC).
See https://pubs.acs.org/sharingguidelines for options on how to legitimately share published articles.

ACS Publications © 2018 American Chemical Society

DOI: 10.1021/acs.jpcc.8b02446
J. Phys. Chem. C 2018, 122, 9611−9618

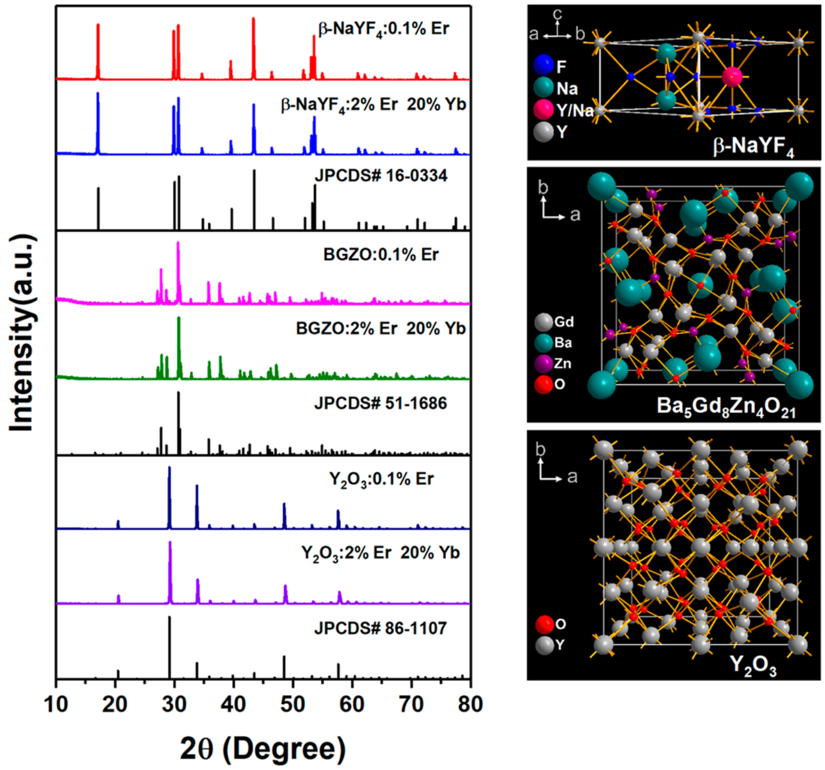

Figure 1. Representative XRD patterns of β-$NaYF_4$, BGZO, and Y_2O_3 and their standard data. Crystal structures of β-$NaYF_4$, BGZO, and Y_2O_3.

state laser materials for high power lasers in the infrared (IR) spectral range.[24−26] A lot of explorations about its UC characteristics indicate that Y_2O_3 is a promising candidate for UC.[27−29] Apart from sesquioxides, some oxide materials with relatively low phonon energies also show efficient UCL.[30−32] Zincate composite ternary oxides exhibit desirable mechanical and optical properties and have had considerable research in the applications of UCL and quantum cutting.[33−37] For instance, $Ba_5Gd_8Zn_4O_{21}$ (BGZO) possessing low phonon energy (472 cm^{-1}) shows efficient red UCL with a UCQY as high as 2.7%.[38,39]

The UC emission color has always been a significant concern due to the potential applications of UCL. For a commonly doped concentration such as 2%Er, 20%Yb, the output color may be different in distinct host matrices. A general rule had been concluded that the red to green (R/G) intensity ratios in oxides were larger than those in fluorides despite the higher red emission efficiencies in the latter.[40] Recently, the emitting color can be modulated between green and red by doping different rare earth ions concentrations, adjusting excitation pulse width and introducing manganese ions.[41−43] Nevertheless, in Er^{3+}/Yb^{3+} doubly doped system, the investigation on the effectiveness of excitation for the red UC emission as a function of phonon energies of host materials is not sufficient.

In the present work, we select β-$NaYF_4$, BGZO, and Y_2O_3 as host materials doped with the same atomic percentage concentration of dopants (e.g., 2%Er, 20%Yb) to investigate the influence of phonon energy on red UC emission intensity. All the samples are bulk phosphors for minimizing the effects caused by surface defects. The excitation processes of the red UC emission in the three UCPs are studied comparably. The upward transition from the Er^{3+} intermediate $^4I_{13/2}$ state to $^4F_{9/2}$ level through phonon-assisted energy transfer from Yb^{3+} is determined to be the dominant excitation mechanism for the red UC emission under low IR excitation densities. A spectroscopic method for evaluating the energy transfer coefficient is proposed. We find that the energy transfer coefficient increases rapidly with the increase of phonon energy, clearly indicating the nature of phonon-assisted energy transfer in the excitation of the red UC. The emission efficiency of the red level is also studied for comprehensively evaluating the performance of the red UC intensity. Our results reveal that the moderate phonon energy of BGZO is in favor of both effective excitation and efficient emission for the red UCL.

2. EXPERIMENTAL SECTION

2.1. Materials and Synthesis. β-$NaYF_4$, BGZO, and Y_2O_3 polycrystalline bulk phosphors samples were fabricated by a simple solid-state reaction method. Generally, high purity materials $BaCO_3$ (A.R.), Gd_2O_3 (99.999%), ZnO (A.R.), Y_2O_3 (99.999%), Er_2O_3 (99.999%), Yb_2O_3 (99.999%), YF_3 (99.9%), ErF_3 (99.9%), YbF_3 (99.99%), and NH_4F (A.R.) were weighted precisely according to certain stoichiometric ratios. The mixtures needed to be thoroughly ground in an agate mortar for 30 min. Subsequently, all these ground powders required further high temperature calcination. BGZO and Y_2O_3 were calcined in air atmosphere for 5 h at 1300 and 1600 °C, respectively. β-$NaYF_4$ powders were sintered at 550 °C for 6 h under the protection of nitrogen stream in a tube furnace. All the as-prepared products were ground into final powders for the following characterization after the furnace cooled down to room temperature.

2.2. Characterization. The crystalline structures of all samples were confirmed by analyzing X-ray power diffraction (XRD) patterns collected on a Bruker D8 Focus diffractometer. The measuring range from 10° to 80° with Cu Ka (λ = 1.540 56 Å) radiation was employed.

DOI: 10.1021/acs.jpcc.8b02446
J. Phys. Chem. C 2018, 122, 9611−9618

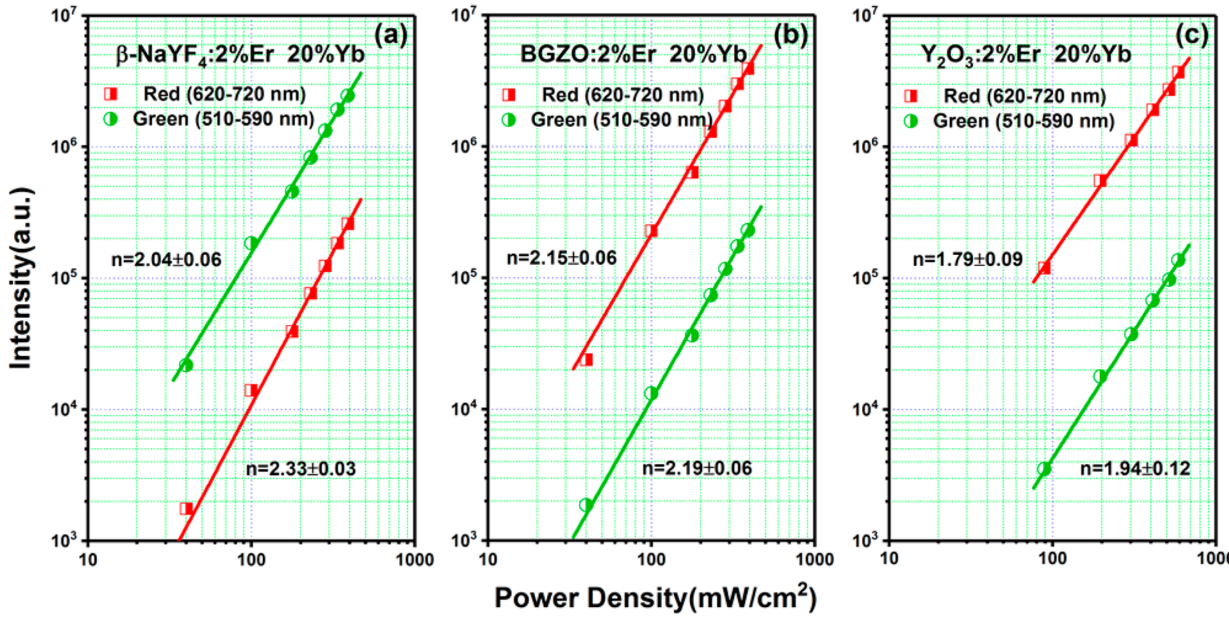

Figure 2. Double logarithmic plots of red and green UC emission intensities versus 980 nm laser power density in (a) β-NaYF$_4$, (b) BGZO, and (c) Y_2O_3.

2.3. Spectroscopy Measurements. Steady state UCL spectra were measured on a FLS920 spectrometer (Edinburgh Instruments) with an external power controllable 980 nm lasers as an excitation source. The photoluminescence (PL) spectra were also detected using the FLS920 spectrometer excited by a xenon lamp. Using an optical parametric oscillator (OPO) as an excitation source, the fluorescence decay curves were measured by applying a Triax550 spectrometer, and the signals were recorded on a Tektronix digital oscilloscope (TDS 3052). All the measurements were developed at room temperature.

3. RESULTS AND DISCUSSION

3.1. Crystal Structure and Purity. The XRD patterns of three kinds of materials with particular doping concentrations are shown in Figure 1. All the diffraction peaks of these samples are in good agreement with their standard patterns, respectively. No extra characteristic peaks from impurities can be observed, indicating that pure phase polycrystalline phosphors have been successfully synthesized by a solid-state reaction. As presented in the right panel of Figure 1, β-NaYF$_4$ has a cation disorder structure and a hexagonal symmetry with a $P\bar{6}$(174) space group. The trivalent Y^{3+} ions occupy two types of cation sites and all of their coordination numbers are nine.[21,23,44] BGZO possesses a tetragonal space group $I4/m$(87), in which two nonequivalent Gd^{3+} ions sites can be found and they are both coordinated with seven oxygen atoms.[35,39] Y_2O_3 crystallizes in the cubic space group $Ia3$(206) and has two six-coordinate sites (C_2, C_{3i}). The optical properties are nearly attributed to doped ions on C_2 sites because of the inversion symmetry of C_{3i} sites.[25,26] The Er^{3+} and Yb^{3+} ions can effectively substitute RE^{3+} sites owing to similar radii and identical valence states.

3.2. Excitation Mechanism and Upconversion Luminescence. Generally, the UCL intensity (I) is proportional to the nth power of the NIR pump power (P): $I \propto P^{n}_{(\mathrm{NIR})}$, where n is the number of pump photons absorbed to excite to the emitting state.[45] The dependence of UCL intensity of these three materials with the same doped concentration were analyzed and plotted in double logarithmic coordinate in Figure 2. All the slopes (n) are close to 2 via linear fitting, signifying a quadratic dependence of both green and red emission on pump power.

The energy level diagram with the predominant transition pathways and energy transfer processes is schematically depicted to comprehend the UC mechanisms in Figure 3.

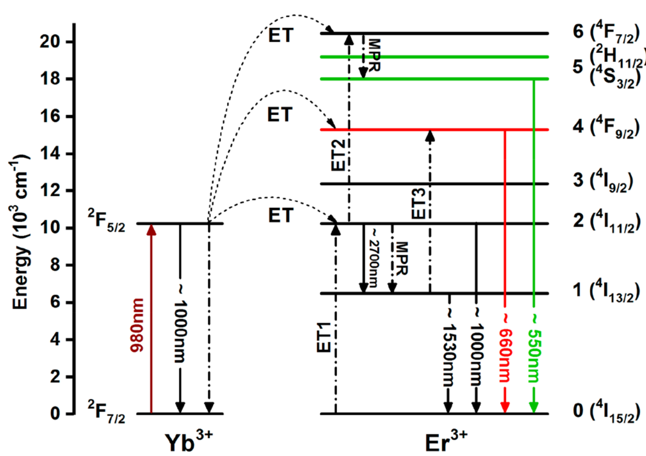

Figure 3. Schematic energy level diagram of UC process and the major transition pathways in Er^{3+}/Yb^{3+} system.

The ground state absorption and excited state absorption of Er^{3+} ions can be neglected due to efficient energy transfer and such a high concentration of sensitizer.[46] Under weak pump power densities excitation, only the processes involving two photons are considered. The green emitting states $^2H_{11/2}$ and $^4S_{3/2}$ can be populated through two-step sequential energy transfer processes (ET1, ET2) followed by a MPR process from the $^4F_{7/2}$ level. The red emitting state $^4F_{9/2}$ may either be populated via MPR from the upper $^4S_{3/2}$ level or energy transfer upconversion (ET3) from the lower $^4I_{13/2}$ level. Besides the visible UC emission, one can observe other characteristic emission peaks centered at 1000 and 1530 nm assigning to the

DOI: 10.1021/acs.jpcc.8b02446
J. Phys. Chem. C 2018, 122, 9611−9618

$^2F_{5/2} \rightarrow {}^2F_{7/2}$ transition of Yb^{3+} and the $^4I_{13/2} \rightarrow {}^4I_{15/2}$ transition of Er^{3+}, respectively (Figure S1). To further explore the influence of MPR on red UCL, the PL and UCL spectra were measured and displayed together in Figure 4. All the

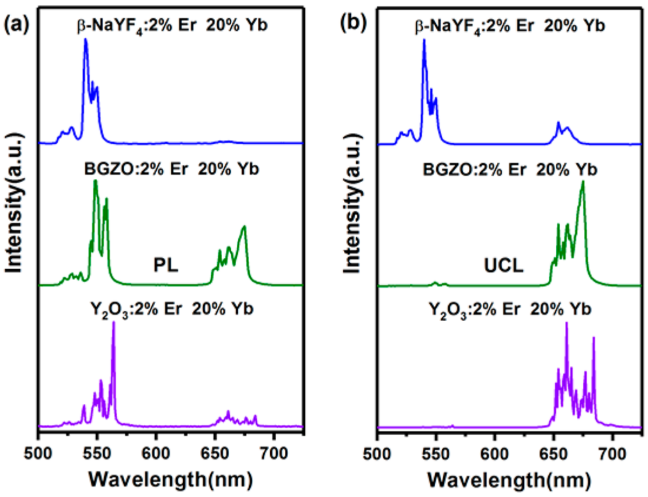

Figure 4. Normalized (a) PL and (b) UCL spectra. The PL spectra were excited by 488 nm using a xenon lamp.

spectra are normalized to their maximum emission peaks. In PL spectra, the $Er^{3+4}F_{7/2}$ state will be directly populated and subsequently relax down to $^2H_{11/2}$ and $^4S_{3/2}$ levels upon 488 nm excitation. Thereby, the red emitting state $^4F_{9/2}$ will be populated exclusively through MPR from green levels. Clearly, the R/G ratios of these three matrices in UCL spectra are larger than those in PL spectra, implying that MPR makes insignificant contribution to the red UCL for all samples.

3.3. Calculating the Emission Efficiencies of the $^4F_{9/2}$ State in Three Materials.

The emission efficiency of red level (η_4) is a crucial parameter for assessing properties of materials to get red UC emission. η_4 can be calculated via the following formula:

$$\eta_4 = \frac{\tau_4}{\tau_{4r}}$$

where τ_4 and τ_{4r} are experimental lifetime and calculated radiative lifetime of $^4F_{9/2}$ state, respectively. The experimental lifetimes in these three samples and the radiative lifetimes in β-$NaYF_4$ and Y_2O_3 can be easily obtained by using the fluorescence decay curves in Figure 5d or from the literature.[47−49] Here, we use a method[49] reported previously by our group to acquire the radiative lifetime of the red level in a BGZO matrix via the combination of PL spectra and time evolutions of 0.1%Er singly doped samples in Figure 5b,c. In Figure 5a, one can observe three emission bands centered at 660, 1000, and 1530 nm assigning to $^4F_{9/2} \rightarrow {}^4I_{15/2}$, $^4I_{11/2} \rightarrow {}^4I_{15/2}$, and $^4I_{13/2} \rightarrow {}^4I_{15/2}$ transitions, respectively. Under the condition of low Er^{3+} concentration, the lower $^4I_{11/2}$ and $^4I_{13/2}$ intermediate levels can be populated through cascade MPR and radiative transitions from upper levels upon 650 nm excitation. In view of the low emission efficiency of red level in oxide and the large radiative branch ratio of $^4F_{9/2} \rightarrow {}^4I_{15/2}$ transition (0.91), the populations of these two lower levels by radiative transitions from $^4F_{9/2}$ can be almost ignored with respect to those through cascade MPR from red state. Thereby, the relatively weak NIR emission intensities indicate a large value of η_4. A much shorter value was achieved to be 353 μs compared to that in another oxide Y_2O_3, which may be caused by the longer RE-O bands and distinct coordination environments. The final results are collected and listed in Table 1. Apparently, η_4 reduced monotonously with the increase of phonon energy of host matrix due to the accelerating of nonradiative transition probability.

3.4. Energy Transfer Coefficient for ET3.

As discussed above, the upward transition (ET3) is the major excitation mechanism for red level. Thereby, this process makes the intensity of the red UC be proportional to the product of the

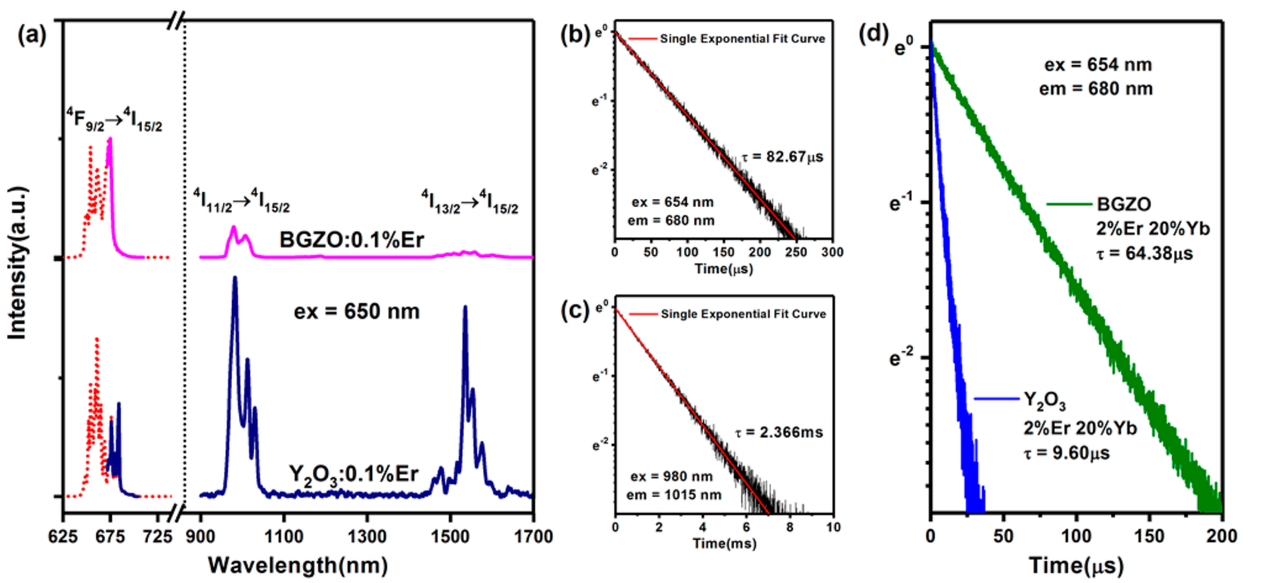

Figure 5. (a) PL spectra of BGZO:0.1%Er and Y_2O_3:0.1%Er upon 650 nm excitation. The full spectra shapes of $^4F_{9/2} \rightarrow {}^4I_{15/2}$ transition are also exhibited as red dashed lines. Two different detectors are employed to detect visible and NIR regions, as indicated by black dashed line, and the red emission integrated intensities are normalized. The fluorescence decay curves of (b) $^4F_{9/2}$ level and (c) $^4I_{11/2}$ level in BGZO:0.1%Er sample. The fluorescence decay curves of (d) $^4F_{9/2}$ level in BGZO:2%Er 20%Yb and Y_2O_3:2%Er, 20%Yb.

DOI: 10.1021/acs.jpcc.8b02446
J. Phys. Chem. C 2018, 122, 9611−9618

Table 1. Parameters for Comparing Properties of Red Upconversion Emission

2%Er 20%Yb	phonon energy (cm^{-1})	τ_{4r} (μs)	τ_4 (μs)	η_4 (%)	C_{d4} (au)	$\eta_4 C_{d4}$ (au)
β-$NaYF_4$	360	1642.04	570.50	34.74	C_0	$0.35C_0$
BGZO	472	353.29	64.38	18.22	$88.84C_0$	$16.19C_0$
Y_2O_3	600	737.53	9.60	1.30	$407.95C_0$	$5.30C_0$

$Yb^{3+2}F_{5/2}$ population and the $Er^{3+4}I_{13/2}$ population based on the theory of energy transfer.[1,50] The proportionality coefficient is directly related to the energy transfer coefficient for the ET3 process. Here, we study the proportional relationships for these three samples in order to achieve their relative coefficients for ET3 to compare the probability of second step energy transfer from $Yb^{3+2}F_{5/2}$ to $Er^{3+4}I_{13/2}$ in three UCPs. For the sample with unit volume, the intensity of the red UC emission (I_4) excited by ET3 can be written as

$$I_4 = \eta_4 C_{d4} n_d n_1$$

where C_{d4} is the coefficient for ET3 from Yb^{3+} in its $^2F_{5/2}$ excited state to Er^{3+} in its $^4I_{13/2}$ excited state and n_d and n_1 are populations of $Yb^{3+2}F_{5/2}$ and $Er^{3+4}I_{13/2}$, respectively. With consideration of excitation energy diffusion among Yb^{3+} ions, the coefficient C_{d4} should be dependent on the Yb^{3+} concentration. However, if the Yb^{3+} concentration is much higher than the Er^{3+} concentration in the case of this work (20 at. %), rapid diffusion energy transfer takes place. Thus, the coefficient C_{d4} is no longer dependent on the Yb^{3+} concentration and takes nearly a constant value.[51,52]

The integrated intensities of $Yb^{3+2}F_{5/2} \rightarrow {}^2F_{7/2}$ emission (I_d) and $Er^{3+4}I_{13/2} \rightarrow {}^4I_{15/2}$ emission (I_1) can be employed to represent n_d and n_1 by $\tau_{dr}I_d$ and $\tau_{1r}I_1$, respectively, with τ_{dr} and τ_{1r} the radiative lifetimes of $Yb^{3+2}F_{5/2}$ and $Er^{3+4}I_{13/2}$. Here, the radiative lifetimes are considered as the fluorescence lifetimes measured in 0.1%Yb singly doped and 0.1%Er singly doped samples (Figure 6) because low doping concentrations and large energy gaps enable the fluorescence lifetimes much close to the radiative lifetimes. To obtain the dependence of I_4 on $\eta_4 n_d n_1$, emission spectra upon 980 nm laser excitation with different pump powers (ranging from 30−110 mW) were measured, as shown in Figure 7. In the measurement, the weights of powders in the sample holder were controlled to make ensure that the identical total volumes of the particles were excited by 980 nm laser for different materials. Meanwhile, the thickness of the sample was as low as 0.1 mm for a uniform excitation density inside the sample. The dependences of I_4 on $\eta_4 n_d n_1$ for these three samples are plotted together in Figure 8, and they all exhibit approximate linear relationships. The small deviations may come from some other mechanisms reported previously.[50,53−55]

It is obvious that the dependences are indeed satisfied with proportional function as expected. The relative value of C_{d4} is the slope of the straight line, as listed in Table 1. Clearly, Y_2O_3 has the largest C_{d4}, which is about 408-fold larger than that in β-$NaYF_4$. It can be found that the coefficient C_{d4} increases dramatically with the increase of phonon energy. It is well understood that ET3 suffers from a large energy mismatch (~1500 cm^{-1}) between the $Yb^{3+2}F_{5/2} \rightarrow {}^2F_{7/2}$ transition and the $Er^{3+4}I_{13/2} \rightarrow {}^4F_{9/2}$ transition. ET3 is therefore a phonon-assisted energy transfer. A higher phonon energy enables a smaller number of phonons to make up the energy mismatch, and hence to speed up energy transfer. Although Y_2O_3 has the largest ET3 coefficient among the three hosts, it also has the shortest $^4F_{9/2}$ lifetime due to high phonon energy induced enhancement of nonradiative relaxation. Certainly, the higher phonon energy also means the faster MPR of the $^4F_{9/2}$ state and it therefore lowers the UCQY of the red UC emission.[56,57] Hence, the comprehensive results indicate that optimization of phonon energy could be more profitable to find efficient red UCPs in Er^{3+}/Yb^{3+} system.

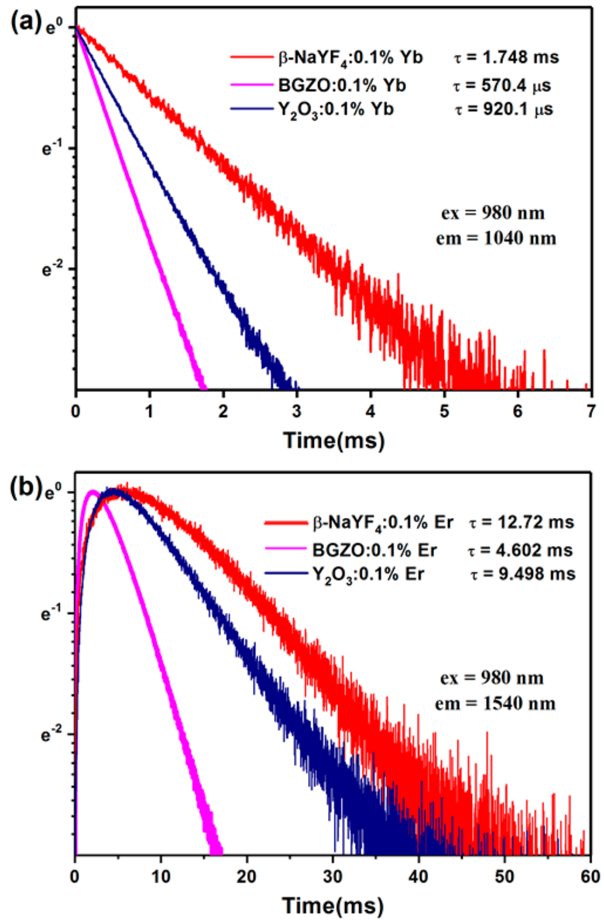

Figure 6. Time evolutions of (a) $Yb^{3+2}F_{5/2}$ and (b) $Er^{3+4}I_{13/2}$ levels in different samples.

The obtained result is similar to a previous report on the energy transfer coefficient in Tm^{3+}/Yb^{3+}-doped oxides and fluorides by Mita and co-workers.[52] They acquired the absolute value of coefficient for only the first step energy transfer via the dependence of $Yb^{3+2}F_{5/2}$ lifetime on donor concentration. However, this method may not be applied to Er^{3+}/Yb^{3+} system or suitable to obtain accurate values other than the first step energy transfer. Here, we use a spectroscopic method for evaluating the relative value of second step energy transfer coefficient in Er^{3+}/Yb^{3+}-doped system. Moreover, our method might be used in Tm^{3+}/Yb^{3+} and Ho^{3+}/Yb^{3+} systems for comparing the second step energy transfer coefficients in different host materials. Apart from the second step energy transfer coefficient and red emission efficiency, some other factors such as absorption strength, quenching concentration,

DOI: 10.1021/acs.jpcc.8b02446
J. Phys. Chem. C 2018, 122, 9611−9618

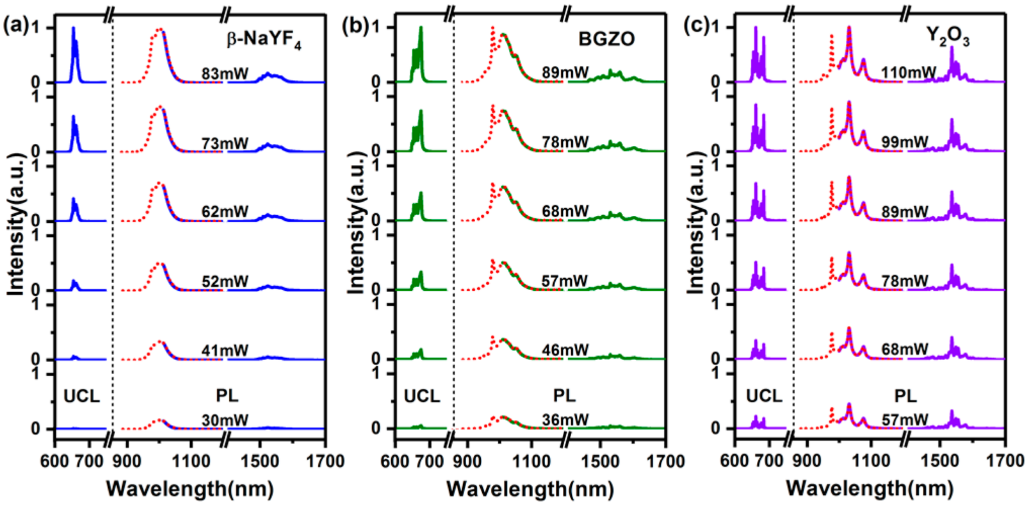

Figure 7. UCL and PL spectra of (a) β-$NaYF_4$, (b) BGZO, and (c) Y_2O_3 with the same doping concentration (2%Er, 20%Yb) under various 980 nm pump powers excitation (solid line). The full spectra shapes of Yb^{3+} emission are also presented (red dashed line). Two different detectors were employed to detect visible and NIR regions, as indicated by black dashed lines. The spectra are normalized for each detector, respectively.

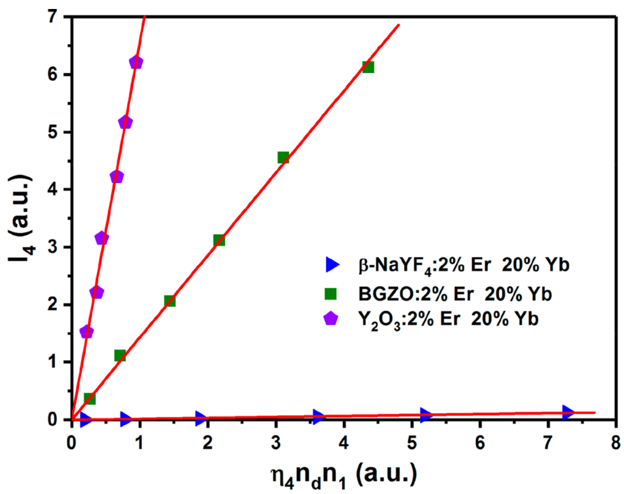

Figure 8. Dependences of the red emission intensities on the product of red level emission efficiency and the populations of $^4I_{13/2}$ of Er^{3+} as well as $^2F_{5/2}$ of Yb^{3+}. The fitting curves (red solid line) given by linear functions are also presented.

spectral overlap, and the population of the $Er^{3+4}I_{13/2}$ level, may also affect the Er^{3+} red UC emission intensity, which are not within the scope of this article.

4. CONCLUSION

Three kinds of efficient UCPs, β-$NaYF_4$, BGZO, and Y_2O_3, were synthesized by a traditional solid state reaction. In the condition of the same doping concentration, they show the same excitation mechanism but different output colors under low density excitation. A spectroscopic method for evaluating the relative second step energy transfer coefficient is proposed. It is revealed that the transfer coefficient in Y_2O_3 is around 4.6-fold and 408-fold larger than that in BGZO and β-$NaYF_4$, respectively, indicating a continuously enhanced excitation of the red emission on increasing phonon energy. The phonon energy dependent behavior essentially reflects the phonon-assisted energy transfer excitation mechanism. This work declares that effective excitation of the red UC requires high phonon energy to make up a large energy mismatch (~1500 cm^{-1}) for minimizing the phonon number. However, with consideration of high phonon energy induced fast nonradiative decay of the red emitting state, optimization of the phonon energy is strongly encouraged for achieving outstanding red UC phosphors based on the Er^{3+}/Yb^{3+} system. Furthermore, the $Er^{3+4}F_{9/2}$ radiative lifetime in the BGZO matrix is evaluated to be 353 μs for the first time. The research means utilized in this work can be widely applicable rather than specific to these three hosts, and we also believe that this spectroscopic method might be extended to Tm^{3+}/Yb^{3+} and Ho^{3+}/Yb^{3+} systems.

■ ASSOCIATED CONTENT

Supporting Information

The Supporting Information is available free of charge on the ACS Publications website at DOI: 10.1021/acs.jpcc.8b02446.

Normalized UCL and PL spectra of β-$NaYF_4$, BGZO, and Y_2O_3 samples upon 980 nm excitation (PDF)

■ AUTHOR INFORMATION

Corresponding Authors

*Z. Hao. E-mail: haozd@ciomp.ac.cn.
*J. Zhang. E-mail: zhangjh@ciomp.ac.cn.

ORCID

Hao Wu: 0000-0002-8396-7393
Liangliang Zhang: 0000-0002-9546-8786
Yu Xiao: 0000-0002-0165-4335

Notes

The authors declare no competing financial interest.

■ ACKNOWLEDGMENTS

This work was partially supported by National Key R&D Program of China (Grant No. 2016YFB0701003, 2016YFB0400605, 2017YFB0403104), National Natural Science Foundation of China (Grant No. 51772286, 51402284 and 11604330).

■ REFERENCES

(1) Auzel, F. Upconversion and Anti-Stokes Processes with f and d Ions in Solids. *Chem. Rev.* **2004**, *104*, 139−174.

(2) Moglia, F.; Müller, S.; Reichert, F.; Metz, P. W.; Calmano, T.; Kränkel, C.; Heumann, E.; Huber, G. Efficient Upconversion-Pumped Continuous Wave Er^{3+}:$LiLuF_4$ Lasers. *Opt. Mater.* **2015**, *42*, 167−173.
(3) Zheng, W.; Huang, P.; Tu, D.; Ma, E.; Zhu, H.; Chen, X. Lanthanide-Doped Upconversion Nano-Bioprobes: Electronic Structures, Optical Properties, and Biodetection. *Chem. Soc. Rev.* **2015**, *44*, 1379−1415.
(4) Tsang, M. K.; Ye, W.; Wang, G.; Li, J.; Yang, M.; Hao, J. Ultrasensitive Detection of Ebola Virus Oligonucleotide Based on Upconversion Nanoprobe/Nanoporous Membrane System. *ACS Nano* **2016**, *10*, 598−605.
(5) Wei, R.; Xi, W.; Wang, H.; Liu, J.; Mayr, T.; Shi, L.; Sun, L. In Situ Crystal Growth of Gold Nanocrystals on Upconversion Nanoparticls for Synergistic Chem-Photothermal Therapy. *Nanoscale* **2017**, *9*, 12885−12896.
(6) Yang, D.; Ma, P.; Hou, Z.; Cheng, Z.; Li, C.; Lin, J. Current Advances in Lanthanide Ion (Ln^{3+})-Based Upconversion Nanomaterials for Drug Delivery. *Chem. Soc. Rev.* **2015**, *44*, 1416−1448.
(7) Deng, R.; Qin, F.; Chen, R.; Huang, W.; Hong, M.; Liu, X. Temporal Full-Colour Tuning through Non-Steady-State Upconversion. *Nat. Nanotechnol.* **2015**, *10*, 237−242.
(8) Pandey, A.; Rai, V. K.; Kumar, V.; Kumar, V.; Swart, H. C. Upconversion Based Temperature Sensing Ability of Er^{3+}-Yb^{3+} Codoped $SrWO_4$: An Optical Heating Phosphor. *Sens. Actuators, B* **2015**, *209*, 352−358.
(9) Liu, Y.; Lu, Y.; Yang, X.; Zheng, X.; Wen, S.; Wang, F.; Vidal, X.; Zhao, J.; Liu, D.; Zhou, Z.; et al. Amplified Stimulated Emission in Upconversion Nanoparticles for Super-Resolution Nanoscopy. *Nature* **2017**, *543*, 229−233.
(10) He, M.; Pang, X.; Liu, X.; Jiang, B.; He, Y.; Snaith, H.; Lin, Z. Monodisperse Dual-Functional Upconversion Nanoparticles Enabled Near-Infrared Organolead Halide Perovskite Solar Cells. *Angew. Chem., Int. Ed.* **2016**, *55*, 4280−4284.
(11) Chen, W.; Joly, A. G.; McCready, D. E. Upconversion Luminescence from CdSe Nanoparticles. *J. Chem. Phys.* **2005**, *122*, 224708.
(12) Joly, A. G.; Chen, W.; McCready, D. E.; Malm, J.; Bovin, J. Upconversion Luminescence of CdTe Nanoparticles. *Phys. Rev. B: Condens. Matter Mater. Phys.* **2005**, *71*, 165304.
(13) Chen, W.; Joly, A. G.; Zhang, J. Z. Up-Conversion Luminescence of Mn^{2+} in ZnS: Mn^{2+} Nanoparticls. *Phys. Rev. B: Condens. Matter Mater. Phys.* **2001**, *64*, 041202.
(14) Sun, L. D.; Wang, Y. F.; Yan, C. H. Paradigms and Challenges for Bioapplication of Rare Earth Upconversion Luminescent Nanoparticles: Small Size and Tunable Emission/Excitation Spectra. *Acc. Chem. Res.* **2014**, *47*, 1001−1009.
(15) Tu, L.; Liu, X.; Wu, F.; Zhang, H. Excitation Energy Migration Dynamics in Upconversion Nanomaterials. *Chem. Soc. Rev.* **2015**, *44*, 1331−1345.
(16) Smith, A. M.; Mancini, M. C.; Nie, S. Bioimaging: Second Window for in Vivo Imaging. *Nat. Nanotechnol.* **2009**, *4*, 710−711.
(17) Pokhrel, M.; kumar Gangadharan, A.; Sardar, D. K. High Upconversion Quantum Yield at Low Pump Threshold in Er^{3+}/Yb^{3+} Doped La_2O_2S Phosphor. *Mater. Lett.* **2013**, *99*, 86−89.
(18) Huang, P.; Zheng, W.; Zhou, S.; Tu, D.; Chen, Z.; Zhu, H.; Li, R.; Ma, E.; Huang, M.; Chen, X. Lanthanide-Doped $LiLuF_4$ Upconversion Nanoprobes for the Detection of Disease Biomarkers. *Angew. Chem., Int. Ed.* **2014**, *53*, 1252−1257.
(19) Lei, P.; An, R.; Yao, S.; Wang, Q.; Dong, L.; Xu, X.; Du, K.; Feng, J.; Zhang, H. Ultrafast Synthesis of Novel Hexagonal Phase $NaBiF_4$ Upconversion Nanoparticles at Room Temperature. *Adv. Mater.* **2017**, *29*, 1700505.
(20) Zhou, J.; Liu, Q.; Feng, W.; Sun, Y.; Li, F. Upconversion Luminescent Materials: Advances and Applications. *Chem. Rev.* **2015**, *115*, 395−465.
(21) Banski, M.; Podhorodecki, A.; Misiewicz, J.; Afzaal, M.; Abdelhady, A. L.; O'Brien, P. Selective Excitation of Eu^{3+} in the Core of Small β-$NaGdF_4$ Nanocrystals. *J. Mater. Chem. C* **2013**, *1*, 801−807.
(22) Boyer, J. C.; van Veggel, F. C. J. M. Absolute Quantum Yield Measurements of Colloidal $NaYF_4$:Er^{3+}, Yb^{3+} Upconverting Nanoparticles. *Nanoscale* **2010**, *2*, 1417−1419.
(23) Renero-Lecuna, C.; Martín-Rodríguez, R.; Valiente, R.; González, J.; Rodríguez, F.; Krämer, K. W.; Güdel, H. U. Origin of the High Upconversion Green Luminescence Efficiency in β-$NaYF_4$:2%Er^{3+}, 20%Yb^{3+}. *Chem. Mater.* **2011**, *23*, 3442−3448.
(24) Zhang, L.; Pan, W. Structural and Thermo-Mechanical Properties of Nd:Y_2O_3 Transparent Ceramics. *J. Am. Ceram. Soc.* **2015**, *98*, 3326−3331.
(25) Kränkel, C. Rare-Earth-Doped Sesquioxides for Diode-Pumped High-Power Lasers in the 1-, 2-, and 3-μm Spectral Range. *IEEE J. Sel. Top. Quantum Electron.* **2015**, *21*, 250−262.
(26) Guzik, M.; Pejchal, J.; Yoshikawa, A.; Ito, A.; Goto, T.; Siczek, M.; Lis, T.; Boulon, G. Structural Investigations of Lu_2O_3 as Single Crystal and Polycrystalline Transparent Ceramic. *Cryst. Growth Des.* **2014**, *14*, 3327−3334.
(27) Lim, S. F.; Riehn, R.; Ryu, W. S.; Khanarian, N.; Tung, C. K.; Tank, D.; Austin, R. H. In Vivo and Scanning Electron Microscopy Imaging of Upconverting Nanophosphors in Caenorhabditis Elegans. *Nano Lett.* **2006**, *6*, 169−174.
(28) Hemmer, E.; Venkatachalam, N.; Hyodo, H.; Hattori, A.; Ebina, Y.; Kishimoto, H.; Soga, K. Upconverting and NIR Emitting Rare Earth Based Nanostructures for NIR-Bioimaging. *Nanoscale* **2013**, *5*, 11339−11361.
(29) Yang, D.; Yang, G.; Wang, X.; Lv, R.; Gai, S.; He, F.; Gulzar, A.; Yang, P. Y_2O_3:Yb,Er@mSiO_2-Cu_xS Double-Shelled Hollow Spheres for Enhanced Chemo-/Photothermal Anti-Cancer Therapy and Dual-Modal Imaging. *Nanoscale* **2015**, *7*, 12180−12191.
(30) Chen, G.; Somesfalean, G.; Liu, Y.; Zhang, Z.; Sun, Q.; Wang, F. Upconversion Mechanism for Two-Color Emission in Rare-Earth-Ion-Doped ZrO_2 Nanocrystals. *Phys. Rev. B: Condens. Matter Mater. Phys.* **2007**, *75*, 195204.
(31) Liu, M.; Gu, M.; Tian, Y.; Huang, P.; Wang, L.; Shi, Q.; Cui, C. Multifunctional $CaSc_2O_4$:Yb^{3+}/Er^{3+} One-Dimensional Nanofibers: Electrospinning Synthesis and Concentration-Modulated Upconversion Luminescent Properties. *J. Mater. Chem. C* **2017**, *5*, 4025−4033.
(32) Etchart, I.; Huignard, A.; Bérard, M.; Nordin, M. N.; Hernández, I.; Curry, R. J.; Gillin, W. P.; Cheetham, A. K. Oxide Phosphors for Efficient Light Upconversion: Yb^{3+} and Er^{3+} Co-Doped Ln_2BaZnO_5 (Ln = Y, Gd). *J. Mater. Chem.* **2010**, *20*, 3989−3994.
(33) Birkel, A.; Mikhailovsky, A. A.; Cheetham, A. K. Infrared to Visible Upconversion Luminescence Properties in the System Ln_2BaZnO_5 (Ln = La, Gd). *Chem. Phys. Lett.* **2009**, *477* (4), 325−329.
(34) Etchart, I.; Bérard, M.; Laroche, M.; Huignard, A.; Hernández, I.; Gillin, W. P.; Curry, R. J.; Cheetham, A. K. Efficient White Light Emission by Upconversion in Yb^{3+}-, Er^{3+}- and Tm^{3+}- Doped Y_2BaZnO_5. *Chem. Commun.* **2011**, *47*, 6263−6265.
(35) Tian, B.; Chen, B.; Tian, Y.; Li, X.; Zhang, J.; Sun, J.; Zhong, H.; Cheng, L.; Fu, S.; Zhong, H.; et al. Excitation Pathway and Temperature Dependent Luminescence in Color Tunable $Ba_5Gd_8Zn_4O_{21}$:Eu^{3+} Phosphors. *J. Mater. Chem. C* **2013**, *1*, 2338−2344.
(36) Xie, J.; Mei, L.; Liao, L.; Guan, M.; Liu, H. Synthesis and Up-Conversion Luminescence Properties of Ho^{3+}, Yb^{3+} Co-Doped $BaLa_2ZnO_5$. *J. Phys. Chem. Solids* **2015**, *83*, 152−156.
(37) Yu, T.; Lin, H.; Yu, D.; Ye, S.; Zhang, Q. Energy Transfer Dynamics and Quantum Yield Derivation of the Tm^{3+} Concentration-Dependent, Three-Photon Near-Infrared Quantum Cutting in La_2BaZnO_5. *J. Phys. Chem. C* **2015**, *119*, 26643−26651.
(38) Mi, C.; Wu, J.; Yang, Y.; Han, B.; Wei, J. Efficient Upconversion Luminescence from $Ba_5Gd_8Zn_4O_{21}$:Yb^{3+}, Er^{3+} Based on a Demonstrated Cross-Relaxation Process. *Sci. Rep.* **2016**, *6*, 22545.
(39) Suo, H.; Guo, C.; Wang, W.; Li, T.; Duan, C.; Yin, M. Mechanism and Stability of Spectrally Pure Green Up-Conversion Emission in Yb^{3+}/Ho^{3+} Co-Doped $Ba_5Gd_8Zn_4O_{21}$ Phosphors. *Dalton Trans.* **2016**, *45*, 2629−2636.

DOI: 10.1021/acs.jpcc.8b02446
J. Phys. Chem. C 2018, 122, 9611−9618

(40) Dong, H.; Sun, L. D.; Yan, C. H. Energy Transfer in Lanthanide Upconversion Studies for Extended Optical Applications. *Chem. Soc. Rev.* **2015**, *44*, 1608−1634.
(41) Vetrone, F.; Boyer, J. C.; Capobianco, J. A.; Speghini, A.; Bettinelli, M. Significance of Yb^{3+} Concentration on the Upconversion Mechanisms in Codoped Y_2O_3:Er^{3+}, Yb^{3+} Nanocrystals. *J. Appl. Phys.* **2004**, *96*, 661−667.
(42) Suo, H.; Guo, C.; Li, T. Broad-Scope Thermometry Based on Dual-Color Modulation Up-Conversion Phosphor $Ba_5Gd_8Zn_4O_{21}$:Er^{3+}/Yb^{3+}. *J. Phys. Chem. C* **2016**, *120*, 2914−2924.
(43) Tian, G.; Gu, Z.; Zhou, L.; Yin, W.; Liu, X.; Yan, L.; Jin, S.; Ren, W.; Xing, G.; Li, S.; et al. Mn^{2+} Dopant-Controlled Synthesis of $NaYF_4$:Yb/Er Upconversion Nanoparticles for in Vivo Imaging and Drug Delivery. *Adv. Mater.* **2012**, *24*, 1226−1231.
(44) Perera, S. S.; Amarasinghe, D. K.; Dissanayake, K. T.; Rabuffetti, F. A. Average and Local Crystal Structure of β-Er:Yb:$NaYF_4$ Upconverting Nanocrystals Probed by X-ray Total Scattering. *Chem. Mater.* **2017**, *29*, 6289−6297.
(45) Pollnau, M.; Gamelin, D. R.; Lüthi, S. R.; Güdel, H. U.; Hehlen, M. P. Power Dependence of Upconversion Luminescence in Lanthanide and Transition-Metal-Ion Systems. *Phys. Rev. B: Condens. Matter Mater. Phys.* **2000**, *61*, 3337.
(46) Suyver, J. F.; Grimm, J.; Krämer, K. W.; Güdel, H. U. Highly Efficient Near-Infrared to Visible Up-Conversion Process in $NaYF_4$:Er^{3+}, Yb^{3+}. *J. Lumin.* **2005**, *114*, 53−59.
(47) Yao, G.; Lin, C.; Meng, Q.; May, P. S.; Berry, M. T. Calculation of Judd-Ofelt Parameters for Er^{3+} in β-$NaYF_4$:Yb^{3+}, Er^{3+} from Emission Intensity Ratios and Diffuse Reflectance Spectra. *J. Lumin.* **2015**, *160*, 276−281.
(48) Sardar, D. K.; Nash, K. L.; Yow, R. M.; Gruber, J. B. Absorption Intensities and Emission Cross Section of Intermanifold Transition of Er^{3+} in Er^{3+}:Y_2O_3 Nanocrystals. *J. Appl. Phys.* **2007**, *101*, 113115.
(49) Wu, H.; Hao, Z.; Zhang, L.; Zhang, X.; Xiao, Y.; Pan, G.; Wu, H.; Luo, Y.; Zhang, L.; Zhang, J. Er^{3+}/Yb^{3+} Codoped Phosphor $Ba_3Y_4O_9$ with Intense Red Upconversion Emission and Optical Temperature Sensing Behavior. *J. Mater. Chem. C* **2018**, *6*, 3459−3467.
(50) Zhang, J.; Hao, Z.; Li, J.; Zhang, X.; Luo, Y.; Pan, G. Observation of Efficient Population of the Red-Emitting State from the Green State by Non-Multiphonon Relaxation in the Er^{3+}-Yb^{3+} System. *Light: Sci. Appl.* **2015**, *4*, e239.
(51) Mita, Y.; Ide, T.; Togashi, M.; Yamamoto, H. Energy Transfer Processes in Yb^{3+} and Tm^{3+} Ion-Doped Fluoride Crystals. *J. Appl. Phys.* **1999**, *85*, 4160−4164.
(52) Mita, Y.; Togashi, M.; Umetsu, Y.; Yamamoto, H. Energy Transfer Processes in Yb^{3+}- and Tm^{3+}- Ion-Doped Oxide and Fluoride Crystals. *Jpn. J. Appl. Phys.* **2001**, *40*, 5925−5929.
(53) Anderson, R. B.; Smith, S. J.; May, P. S.; Berry, M. T. Revisiting the NIR-to-Visible Upconversion Mechanism in β-$NaYF_4$:Yb^{3+}, Er^{3+}. *J. Phys. Chem. Lett.* **2014**, *5*, 36−42.
(54) Xu, D.; Liu, C.; Yan, J.; Yang, S.; Zhang, Y. Understanding Energy Transfer Mechanisms for Tunable Emission of Yb^{3+}-Er^{3+} Codoped GdF_3 Nanoparticles: Concentration-Dependent Luminescence by Near-Infrared and Violet Excitation. *J. Phys. Chem. C* **2015**, *119*, 6852−6860.
(55) Hyppänen, I.; Höysniemi, N.; Arppe, R.; Schäferling, M.; Soukka, T. Environmental Impact on the Excitation Path of the Red Upconversion Emission of Nanocrystalline $NaYF_4$:Yb^{3+}, Er^{3+}. *J. Phys. Chem. C* **2017**, *121*, 6924−6929.
(56) Miyakawa, T.; Dexter, D. L. Phonon Sidebands, Multiphonon Relaxation of Excited States, and Phonon-Assisted Energy Transfer between Ions in Solids. *Phys. Rev. B: Condens. Matter Mater. Phys.* **1970**, *1*, 2961−2969.
(57) Zhang, Q. Y.; Huang, X. Y. Recent Progress in Quantum Cutting Phosphors. *Prog. Mater. Sci.* **2010**, *55*, 353−427.
(58) Ge, X.; Liu, J.; Sun, L. Controlled Optical Characteristics of Lanthanide Doped Upconversion Nanoparticls for Emerging Applications. *Dalton Trans.* **2017**, *46*, 16729−16737.
(59) Sun, L.; Wei, R.; Feng, J.; Zhang, H. Tailored Lanthanide-Doped Upconversion Nanoparticles and Their Promising Bioapplication Prospects. *Coord. Chem. Rev.* **2018**, *364*, 10−32.

DOI: 10.1021/acs.jpcc.8b02446
J. Phys. Chem. C 2018, 122, 9611−9618